

# Microwave-assisted synthesis of iron oxide nanoparticles in biocompatible organic environment

Cite as: AIP Advances 8, 048201 (2018); <https://doi.org/10.1063/1.4994057>

Submitted: 03 July 2017 • Accepted: 11 August 2017 • Published Online: 13 October 2017

E. Aivazoglou,  E. Metaxa and E. Hristoforou

## COLLECTIONS

Paper published as part of the special topic on [23rd Soft Magnetic Materials Conference](#)



View Online



Export Citation



CrossMark

## ARTICLES YOU MAY BE INTERESTED IN

[Co-precipitation synthesis of magnetic nanoparticles for efficient removal of heavy metal from synthetic wastewater](#)

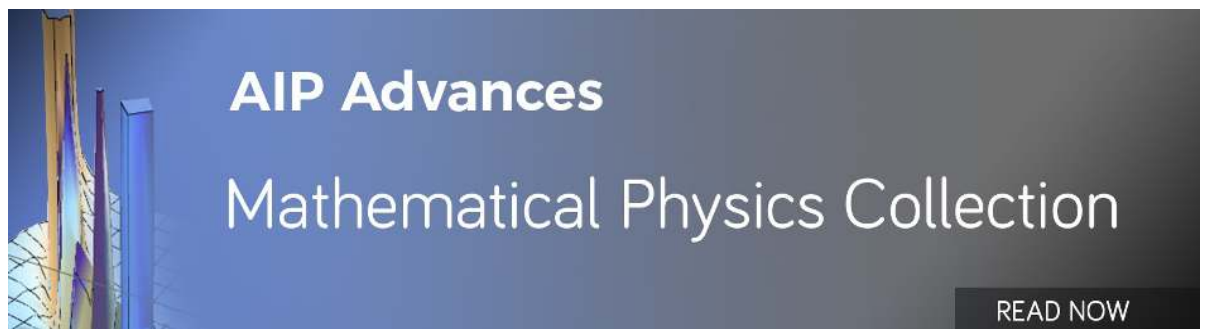
AIP Conference Proceedings **2124**, 020019 (2019); <https://doi.org/10.1063/1.5117079>

[Green synthesis of nanoparticles: Their advantages and disadvantages](#)

AIP Conference Proceedings **1724**, 020048 (2016); <https://doi.org/10.1063/1.4945168>

[Synthesis and characterization of Fe<sub>2</sub>O<sub>3</sub> nanoparticles by simple precipitation method](#)

AIP Conference Proceedings **1724**, 020064 (2016); <https://doi.org/10.1063/1.4945184>



AIP Advances  
Mathematical Physics Collection

READ NOW

## Microwave-assisted synthesis of iron oxide nanoparticles in biocompatible organic environment

E. Aivazoglou,<sup>a</sup> E. Metaxa, and E. Hristoforou

*Laboratory of Electronic Sensors, National Technical University of Athens, Zografou Campus, 15780 Athens, Greece*

(Received 3 July 2017; accepted 11 August 2017; published online 13 October 2017)

The development of magnetite and maghemite particles in uniform nanometer size has triggered the interest of the research community due to their many interesting properties leading to a wide range of applications, such as catalysis, nanomedicine-nanobiology and other engineering applications. In this study, a simple, time-saving and low energy-consuming, microwave-assisted synthesis of iron oxide nanoparticles, is presented. The nanoparticles were prepared by microwave-assisted synthesis using polyethylene glycol (PEG) or PEG and  $\beta$ -cyclodextrin ( $\beta$ -CD)/water solutions of chloride salts of iron in the presence of ammonia solution. The prepared nano-powders were characterized using X-Ray Diffraction (XRD), Transition Electron Microscopy (TEM), Fourier-transform Infrared Spectroscopy (FTIR), Raman Spectroscopy, Vibrating Sample Magnetometer (VSM), X-Ray Photoelectron Spectroscopy (XPS) and Thermal analysis (TG/DSC). The produced nanoparticles are crystallized mostly in the magnetite and maghemite lattice exhibiting very similar shape and size, with indications of partial PEG coating. Heating time, microwave power and presence of PEG, are the key factors shaping the size properties of nanoparticles. The average size of particles ranges from 10.3 to 19.2 nm. The nanoparticles exhibit a faceted morphology, with zero contamination levels. The magnetic measurements indicate that the powders are soft magnetic materials with negligible coercivity and remanence, illustrating super-paramagnetic behavior. © 2017 Author(s). All article content, except where otherwise noted, is licensed under a Creative Commons Attribution (CC BY) license (<http://creativecommons.org/licenses/by/4.0/>). <https://doi.org/10.1063/1.4994057>

### I. INTRODUCTION

Iron oxide nanoparticles have triggered the interest of the research community and industry, due to their great variety of applications. Iron oxide nanoparticles, with magnetite ( $\text{Fe}_3\text{O}_4$ ) and maghemite ( $\gamma\text{-Fe}_2\text{O}_3$ ) playing the leading role, find great use in pharmacy and nanomedicine, and are used in cell separation,<sup>1</sup> as MRI contrasting agents,<sup>2</sup> as drug carriers for targeted cancer therapy<sup>3</sup> and as magnetic nanomarkers for pathogens diagnosis using microfluidic sensors<sup>4,5</sup> or magnetic microchips.<sup>6,7</sup> In the environmental sector iron oxide nanoparticles facilitate the purification of polluted water and soil,<sup>8</sup> whereas in the field of energy storage, magnetite nanoparticles are highlighted as a promising anode material for lithium ion batteries.<sup>9</sup> BioMEMS<sup>10,11</sup> are also employing magnetic nanoparticles for implementing lab-on-a-chip applications.

Chemical composition, morphology and size control of nanoparticles are strongly dependent parameters on the method of preparation and play a significant role for engineering applications. Various techniques have been used to synthesize magnetic iron oxides nanoparticles, such as coprecipitation,<sup>12,13</sup> thermal decomposition,<sup>14,15</sup> microemulsion technique,<sup>16</sup> and hydrothermal methods,<sup>17,18</sup> but they all suffer from serious drawbacks such as broad size distribution, long reaction time, low efficiency and need of high temperature and pressure respectively.

<sup>a</sup>Corresponding author: [el.aivazog@gmail.com](mailto:el.aivazog@gmail.com)



The need of a rapid, simple and efficient preparation method that produces monodispersed nanoparticles with good magnetic properties under moderate temperature, led the scientific research on the exploration of microwave-assisted synthetic routes. Since the late 1980s, microwave-assisted synthesis has been utilized in the preparation of organics, organometallics and peptides and only the last couple of decades, the exploration of this method has been introduced in the field of inorganic material synthesis.<sup>19</sup> Various research groups have focused their interest on the microwave-assisted synthesis of magnetite and maghemite. A striking benefit of the microwave-assisted synthesis, which strongly differentiates this method from the classic ones, is the reduced reaction time as well as the homogenous heat supply due to the almost instantaneous interaction of the electromagnetic field with the material being processed rather than surface heating.<sup>20</sup>

Khollam et al.<sup>21</sup> prepared magnetite powders with average crystallite size around 34 nm, using as precursors ferrous sulfate and sodium hydroxide, in the temperature range of 90 - 200°C, using microwave-assisted conditions. Caillot et al.<sup>22</sup> used alcoholic solutions of ferrous chloride and sodium ethoxide solutions heated at about 160°C, using microwave-assisted conditions, resulting in hematite, spinel phase (maghemite) and iron-magnetite nanocomposites, with grain sizes close to 20 nm for magnetite and 60 nm for metallic iron. Monodisperse magnetite nanoparticles (~6nm) were synthesized by microwave-assisted heating at 220°C for 5 min and 250°C for another 5 min, using Fe(acac)<sub>3</sub> and 1,2-hexadecanediol in dibenzyl ether in the presence of oleic acid and [bmim][BF<sub>4</sub>].<sup>23</sup> Hong et al.<sup>24</sup> prepared magnetite nanoparticles with average size of 8-9 nm using ferrous and ferric salts and ammonia occupying a domestic oven without any temperature control. Magnetite nanoparticles of average size around 15-20 nm, with partial surface oxidation to maghemite, were obtained via microwave heating of chloride ferrous salts and NaOH/hydrate hydrazine solution, at 100°C for 120 min.<sup>25</sup> Another research group prepared super-paramagnetic maghemite nanoparticles with mean diameter about 6 nm, by heating under microwave irradiation a solution of iron (III) acetylacetonate and benzyl alcohol at 60°C for 5 min followed by heating at 180°C for 10 min.<sup>26</sup> Komarneri and his co-workers used chloride salts of iron and different alkaline sources (such as ammonia solution NH<sub>4</sub>OH, NaOH, Na<sub>2</sub>CO<sub>3</sub>) under microwave heating at 80-150°C for 1-16min, producing magnetite nanoparticles, with size varying from 24 nm to greater than 1000 nm and saturation magnetization from 59 to 89 emu/g. Their study shows that magnetite's crystallinity increases with increasing temperature of microwave heating.<sup>27</sup>

The addition of polyethylene glycol (PEG) in the precursor mixture, is a condition investigated by several researchers. Polyethylene glycol is a hydrophilic, water-soluble, biocompatible organic polymer. Moreover its high polarizability makes it an excellent microwave-absorbing agent, resulting to the high heating rate and significantly shorten reaction time.<sup>28</sup> Wang et al. synthesized magnetite and hematite ellipsoid-like nanoparticles using ferric chloride, polyethylene glycol (PEG-20000) and hydrazine under microwave-assisted conditions at 100°C for 10 min.<sup>28</sup> Another research group investigated the synthesis of porous magnetite, emphasizing on the influence of the water/PEG ratio to the surface modification.<sup>29</sup> There is also interest on the influence of PEG on the shape of nanoparticles, as absorption of PEG on the nanoparticles surface leads to anisotropic growth, resulting in nanowires.<sup>9,30</sup> The second organic reagent, is  $\beta$ -cyclodextrin.  $\beta$ -cyclodextrin ( $\beta$ -CD) is a cyclic oligosaccharide consisting of seven glucose units with lipophilic central cavities and a hydrophilic outer surface. Its improving properties on solubility, stability, and bioavailability of hydrophobic and biomolecular drugs, have been exploited for pharmaceutical uses.<sup>31</sup>

In this paper, we report a facile, rapid, reproducible and effective method of microwave-assisted synthesis of magnetite and maghemite nanoparticles and investigate the effects of time, microwave power and ammonia concentration on the properties of nanoparticles. The presence of PEG and CD during the microwave radiation was selected in order to evaluate their surface modification properties and their operation not only as binders facilitating the nanoparticles formation, but also as sacrificial agents protecting nanoparticles from oxidation as well as polymeric partial coatings.

## II. EXPERIMENTAL

### A. Materials

The following chemicals were used during the synthetic routes: ferric chloride ( $\text{FeCl}_2 \cdot 4\text{H}_2\text{O}$  (s),  $\text{FeCl}_3 \cdot 6\text{H}_2\text{O}$  (s), aqueous ammonia  $\sim 18\text{M}$  (28-30% w/w), polyethylene glycol-200 (PEG-200) (l), polyethylene glycol-400 (PEG-400) (l),  $\beta$ -cyclodextrin ( $\beta$ -CD) (s) and ethyl alcohol absolute. All the chemicals were analytical grade and used without any further purification. Throughout all the experiments deionized water was used.

### B. Microwave-assisted synthesis of magnetic iron oxide nanoparticles

The microwave-assisted synthesis of the nanoparticles without using any organic reagents was as follows:  $\text{FeCl}_2 \cdot 4\text{H}_2\text{O}$  (0.86 g) and  $\text{FeCl}_3 \cdot 6\text{H}_2\text{O}$  (2.36 g) were dissolved in 40 mL of, preheated at 80-90°C, deionized water in a beaker. In the beaker and under continuous stirring ammonia solution was added, leading to the colour change of the solution from bright orange to dark brown or black. Three different ammonia concentrations were tested: 0.5 M, 0.8 M and 1.1 M. The precursor suspension was heated by microwave. The experimental conditions are shown on TABLE I.

The microwave-assisted synthesis of the nanoparticles using PEG-200 (PEG-400) was as follows: the ferrous solution was prepared like before. In another beaker 40 mL of deionized water were mixed with 32.08 g PEG-200 (PEG-400) and ammonia solution (again the same three different ammonia concentrations were tested). Under continuous stirring and heating at 80-90°C, the above alkaline solution was mixed with the ferrous solution. The solution turned from bright orange to black. After mixing the precursors, the solution was heated by microwave-assisted conditions as shown on TABLE II.

The microwave-assisted synthesis of the nanoparticles using PEG-200 and  $\beta$ -CD was as follows: the ferrous solution was prepared as described above with the addition of 0.108 g  $\beta$ -CD. In another beaker 40 mL of deionized water were mixed with 31.75 g PEG-200 and 3.2 mL ammonia solution. The ferrous solution was then added to the PEG/ammonia solution and the mixture was heated by microwaves at minimum power for 2.5 min.

After the microwave-assisted heating, a black precipitate was collected. All products were washed with deionized water and absolute ethanol twice, and then dried at 80°C for 6h under partial vacuum prior to characterization by different techniques. The microwave oven used for sample preparation was a domestic microwave oven (Bluesky MOF800L.20.1), with maximum power at 800 W and microwave frequency at 2450 MHz.

### C. Characterization methods

The crystallographic structure of the samples was investigated with X-ray diffraction (XRD) measurements, which were carried out with a Bruker AXS D8 Advance Diffractometer, using  $\text{CuK}\alpha_1$

TABLE I. Experimental condition of nanoparticles synthesis without use of organic reagents.

Microwave Power (W)	Time (min)
400	2.5
600	2.5
800	2.5

TABLE II. Experimental conditions of PEG-assisted synthesis.

Microwave Power (W)	Time (min)
400	1 2.5 5
600	1 2.5 5
800	1 2.5 5

radiation in the  $2\theta$  range of  $20^\circ$  to  $110^\circ$ . The average crystallite size  $D$  was calculated from Debye-Scherrer equation using the peaks from  $30^\circ$  to  $50^\circ$ , i.e.  $D = k\lambda/\beta \cos \theta$ , where  $k$  = constant,  $\lambda$  = X-ray wavelength and  $b$  = Full Width at Half Maximum.

The morphology of the nanoparticles was investigated by Transmission Electron Microscopy (TEM) using a JEOL 2000FX operating at 200 kV; diffraction patterns were taken at camera length of 100 cm. Images were recorded by Gatan Erlanshen 500W side-mounted CCD camera and processed using Gatan Microscopy Suite - Digital Micrograph. Samples for TEM were prepared both by gentle deposition of minute amounts of the particles directly onto the surface of a carbon-film covered grid or were previously dispersed in 1mL of chloroform and the flask was sonicated for 2-3 minutes. After sonication a drop of the dispersion has been put on the carbon-film grid. This procedure allowed the better separation of agglomerations in individual particles for easier observation and size quantification of them.

In order to evaluate the organic content of the samples several techniques were used. Raman measurements were carried out in a Renishaw Ramascope RM1000 which is set up with a 632.8 nm He-Ne laser and a Leica DM LM microscope. The entrance slit to the spectrometer was set to 50  $\mu\text{m}$ , the grating at 1800 lines/mm, and the CCD camera was cooled with Peltier plates. For the analysis, a lens with a magnification of  $\times 20$  was used, with a laser beam diameter on the focus point smaller than 2  $\mu\text{m}$  and energy smaller than 5 mW. This was done so that the noise of the machine in the final spectra can be reduced. The range of wavenumbers that was studied was between 150  $\text{cm}^{-1}$  and 2000  $\text{cm}^{-1}$  and the results were acquired using Renishaw "Wire 3.1" which is controlled through the GRAMS32 software. Fourier transform infrared spectra (FTIR) between 4000  $\text{cm}^{-1}$  and 400  $\text{cm}^{-1}$  were carried out on a PerkinElmer Spectrum 100, using a KBr disk method. X-ray photoelectron spectroscopy (XPS) was performed on a KRATOS AXIS ULTRA<sup>DLD</sup> using monochromatic  $\text{AlK}\alpha$  radiation (at 15 kV and 10 mA). The samples were mounted on a steel bar using double sided C tape and inserted into the spectrometer fast entry lock until a vacuum level of approximately  $5 \times 10^{-7}$  mbar was established. The samples were thereafter transferred into the analysis chamber for XPS analysis. For the survey and high resolution scans, pass energies of 160 and 20 eV were used respectively. Survey and high resolution scans were acquired using a step size of 1 and 0.1 eV respectively. Charge neutralization was applied to compensate for surface charging effects. The spectra were acquired at a zero angle of emission (normal emission). Owing to the magnetic nature of the samples the XPS analysis was performed with the analyser in the electrostatic mode. The spectra were energy corrected by placing the C 1s for adventitious carbon (C-C/C-H) at 284.8 eV. The vacuum in the analysis chamber during analysis was  $2-3 \times 10^{-9}$  mbar. Data analysis was performed using the software CasaXPS. Thermogravimetric tests were carried out using a SETARAM-LabSys Instrument. Approximately 100 mg of each material were submitted to a temperature ramp from  $25^\circ\text{C}$  to  $700^\circ\text{C}$  at a heating rate of  $10^\circ\text{C}/\text{min}$  under argon atmosphere. Last but not least, a vibrating sample magnetometer was used to evaluate the magnetic properties at room temperature.

### III. RESULTS AND DISCUSSION

The samples IDs for all the investigated samples and their fabrication conditions are demonstrated on Table III.

#### A. X-ray diffraction patterns

All XRD patterns show low peak intensity and broadening of the peaks, which are characteristics of nanosized crystalline particles. The nanopowders, as it will be presented in the following patterns, all belong to the spinel phases of magnetite ( $\text{Fe}_3\text{O}_4$ ) or/and maghemite ( $\gamma\text{-Fe}_2\text{O}_3$ ). It is important, however, to mention that these two phases are not perfectly distinguishable from the obtained XRD patterns.

In Fig. 1, the X-ray diffraction of the sample prepared without use of PEG (sample A) shows slightly sharper peaks, whereas the addition of PEG (sample C) during the synthesis results to the slight reduction of the peaks intensity and their broadening.

TABLE III. Samples IDs and fabrication conditions.

Sample ID	Use of PEG (Y: Yes, N: No)	Ammonia Concentration (M)	Microwave Power (W)	Time (min)
A	N	0.5	400	2.5
B	Y	0.5	400	1
C	Y	0.5	400	2.5
D	Y	0.5	400	5
E	Y	0.5	600	2.5
F	Y	0.5	800	1
G	N	0.8	400	2.5
H	Y	0.8	400	1
I	Y	0.8	400	2.5
J	Y	0.8	400	5
K	Y	0.8	600	2.5
L	Y	0.8	800	1
M	N	1.1	400	2.5
N	Y	1.1	400	1
O	Y	1.1	400	2.5
P	Y	1.1	400	5
Q	Y	1.1	600	2.5
R	Y	1.1	800	1
S	PEG-400	0.8	400	2.5
T	PEG-400	0.8	400	5
U	PEG-200 + $\beta$ -CD	1.1	400	5

The XRD patterns of samples prepared using PEG-200 in comparison with those prepared under the same conditions but using PEG-400 instead, are illustrated in Fig. 2. The patterns show slight differences of the peaks intensity.

The comparison of the XRD patterns (Fig. 3) of the samples prepared under maximum microwave power for 1 min for different ammonia concentrations, show no major difference.

Regarding the comparison of XRD patterns of samples prepared in the presence of PEG-200 and those prepared in the presence of PEG-200 and  $\beta$ -CD (Fig. 4), no major difference is observed.

Using the Debye-Scherrer equation the average crystallite sizes of the samples were calculated. The results are presented on TABLE IV.

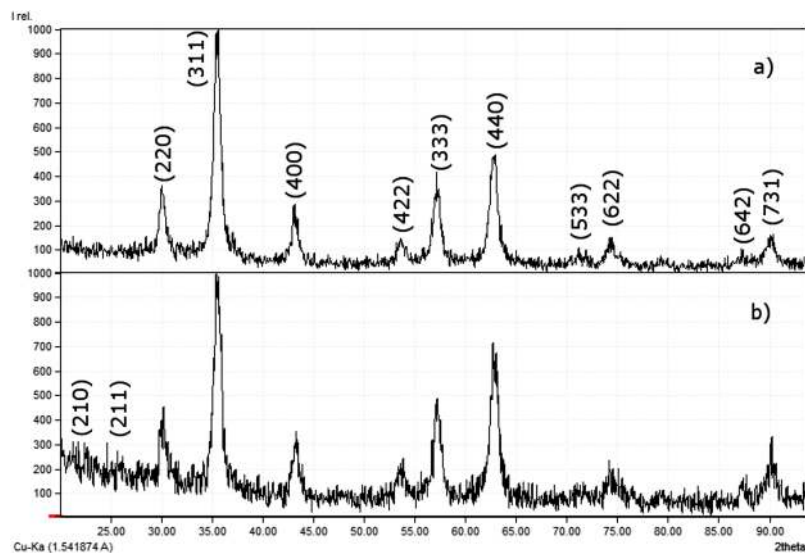


FIG. 1. XRD patterns of nanoparticles prepared a) with use of PEG-200 (sample C) and b) without use of PEG-200 (sample A).

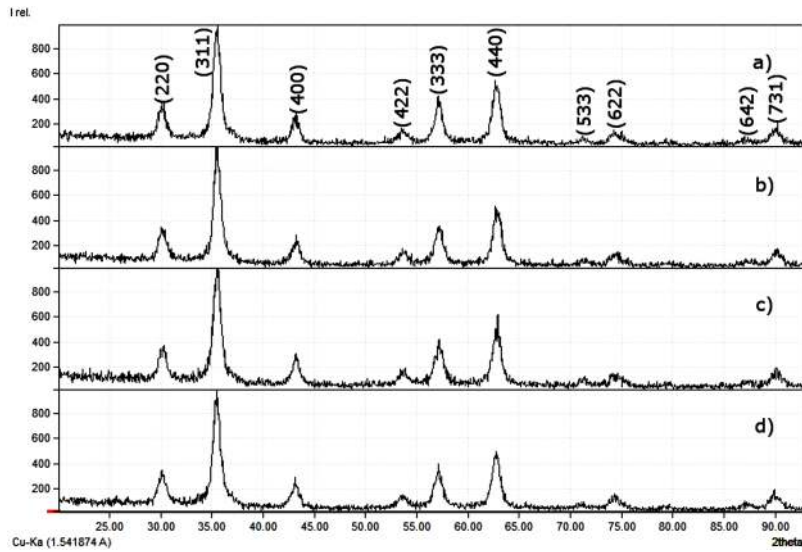


FIG. 2. XRD patterns of nanoparticles prepared a) in the presence of PEG-200 for 5' @400 W (sample J) b) in the presence of PEG-400 for 5' @400 W (sample T) c) in the presence of PEG-200 for 2.5' @400 W (sample I) d) in the presence of PEG-400 for 2.5' @400 W (sample S).

From TABLE IV, it is observed that the average crystallite size of the samples prepared under microwave-assisted heating, ranges from 10.3 nm to 19.2 nm in all different preparation processes. The average crystallite size for each process will be illustrated in the next Chapter, concerning transmission electron microscopy studies.

## B. Transmission electron microscopy images

TEM was used to characterize the size and shape of the iron oxide nanoparticles. Fig. 5 demonstrates the morphology obtained with the different synthetic routes. The PEG-free synthetic

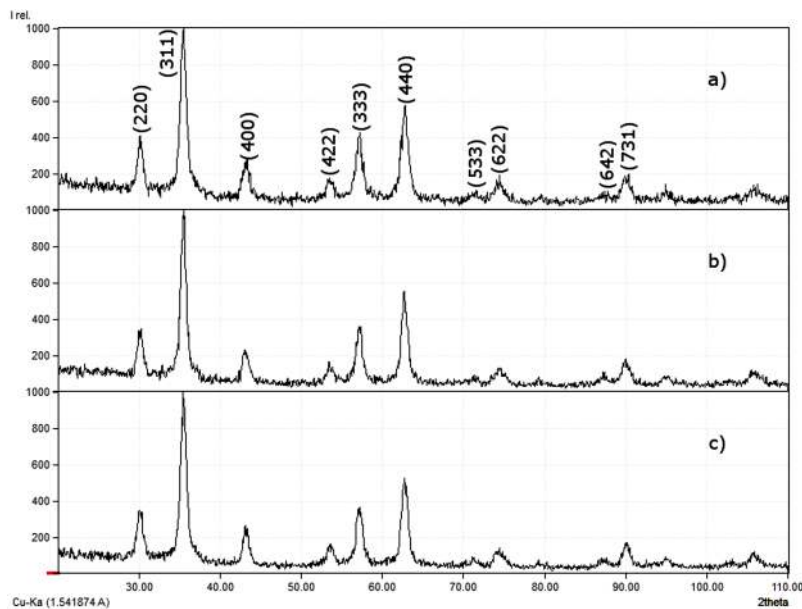


FIG. 3. XRD patterns of nanoparticles prepared in the presence of PEG-200 for 1min@800 W with ammonia concentrations at a) 0.5M (sample F) b) 0.8M (sample L) c) 1.1M (sample R).

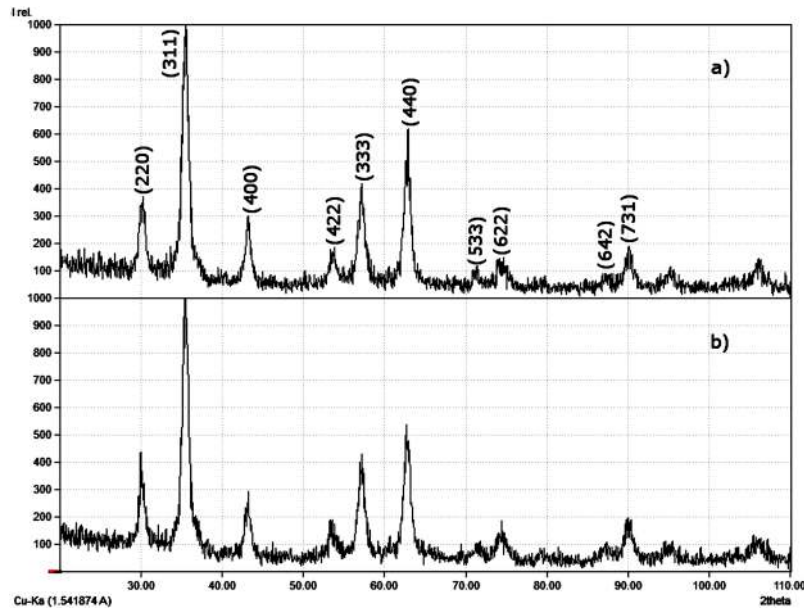


FIG. 4. XRD patterns of nanoparticles prepared in the presence of a) PEG-200 (sample P) and b)  $\beta$ -CD and PEG200 (sample U).

route (sample G) resulted to nanoparticles of  $9.7 \text{ nm} \pm 2.3 \text{ nm}$ , as calculated from a population of 80 particles (Fig. 5 (a)). The PEG-assisted synthesis (sample I) resulted to nanoparticles of  $8.5 \text{ nm} \pm 0.5 \text{ nm}$ , as calculated from a population of 50 particles (Fig. 5 (b)). The histograms beneath each image in Fig. 5 provide a look at the entire population distribution of the nanoparticles diameters used to calculate the mean size  $\pm$  one standard deviation. However, it should be noted that the abnormal size distribution is attributed to the shadow effect of several nanoparticles superimposed one another, eventually permitting electron transmission through them.

TABLE IV. Average crystallite sizes of the samples, calculated with Debye - Scherrer equation.

Sample ID	Average Crystallite Size (nm)
A	13.4
B	11.6
C	11.6
D	15.7
E	13.4
F	15.8
G	13.3
H	11.6
I	10.3
J	15.8
K	15.8
L	19.2
M	16.2
N	10.3
O	15.7
P	19.2
Q	11.6
R	11.6
S	15.8
T	13.3
U	11.7



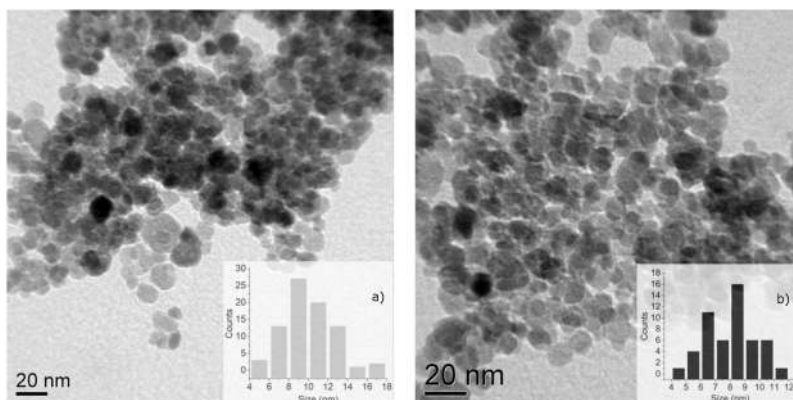


FIG. 5. Representative TEM images of nanoparticles prepared in the a) absence of PEG and b) in the presence of PEG.

### C. Raman spectra

Raman measurements were carried out firstly to evaluate the presence of organic reagents and secondly to obtain a better insight of the participating phases in the samples. Representative spectra of samples prepared with and without PEG-assistance are illustrated in Fig. 6. The presence of a sharper peak at  $510\text{ cm}^{-1}$  and a small shoulder at the range of  $1000\text{--}1250\text{ cm}^{-1}$  at the spectra of PEG-assisted prepared samples, could be an indication of PEG presence at the final products. According to reported results<sup>32–34</sup> there was a typical peak near  $670\text{ cm}^{-1}$  for magnetite, maghemite appeared in four peaks around  $500\text{ cm}^{-1}$ ,  $510\text{ cm}^{-1}$ ,  $645\text{ cm}^{-1}$  and  $1400\text{ cm}^{-1}$ , goethite appeared a peak near  $387\text{ cm}^{-1}$ , while hematite appeared in three peaks at  $220\text{ cm}^{-1}$ ,  $286\text{ cm}^{-1}$  and  $1300\text{ cm}^{-1}$ . The presence of hematite and part of maghemite is attributed to the phase transformation of the analyzed powders, as a consequence of laser-induced thermal effects. It is well known that under heat treatment, magnetite, which shows great light absorbance in the range of wavelengths used in Raman measurements, easily transforms into the oxidized crystal of maghemite at around  $200^\circ\text{C}$  to finally complete oxidation to hematite ( $\alpha\text{-Fe}_2\text{O}_3$ ) at around  $400^\circ\text{C}$ . Shebanova et al., also mention that the rate of the laser-induced transformation is fast enough to be completed even at low temperatures, when the size of the particles is less than  $300\text{ \AA}$ .<sup>34</sup>

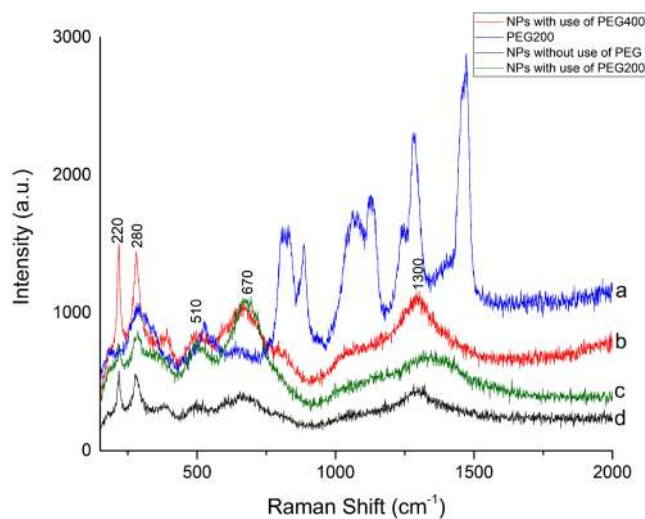


FIG. 6. Raman spectra of a) PEG-200 and nanoparticles prepared b) in the presence of PEG-400 (sample S), c) in the presence of PEG-200 (sample I) and d) in the absence of PEG (sample G).

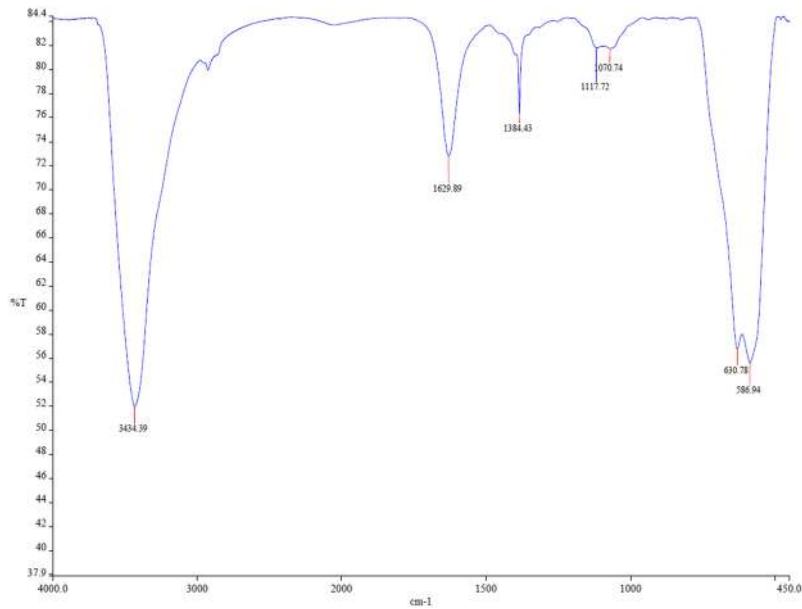


FIG. 7. FT-IR spectra of PEG-assisted prepared nanoparticles.

#### D. Fourier transformation infrared spectra

In order to better evaluate the presence of PEG at PEG-assisted prepared samples, FT-IR spectra were obtained. Representative spectra of a sample prepared using and not using PEG are illustrated in Figures 7 and 8 respectively. The first spectra shows bands at 3434.39 cm<sup>-1</sup>, 1629.89 cm<sup>-1</sup>, 1384.43 cm<sup>-1</sup>, 1117.72 cm<sup>-1</sup>, 1070.74 cm<sup>-1</sup>, 630.78 cm<sup>-1</sup> και 586.94 cm<sup>-1</sup>. The second spectra shows bands at 3429.76 cm<sup>-1</sup>, 1630.79 cm<sup>-1</sup>, 1384.39 cm<sup>-1</sup>, 1115.79 cm<sup>-1</sup>, 1052.64 cm<sup>-1</sup>, 630.88 cm<sup>-1</sup> και 586.93 cm<sup>-1</sup>. The peak at 586.93 cm<sup>-1</sup> is characteristic of magnetite and concerns the Fe-O bending vibration.<sup>35</sup> This peak has strong intensity suggesting high crystallinity of the sample. It must

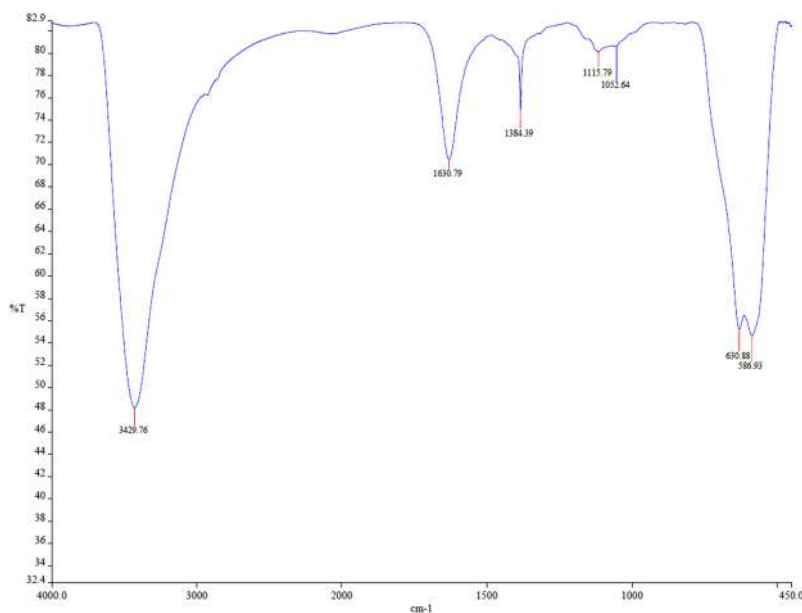


FIG. 8. FT-IR spectra of PEG-free prepared nanoparticles.

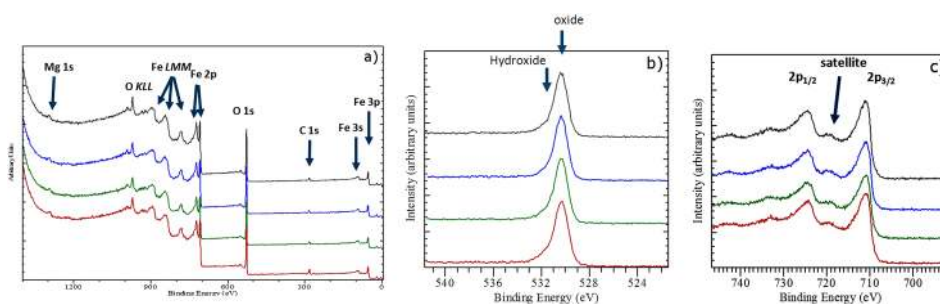


FIG. 9. Representative XPS spectra of nanoparticles prepared in the presence of PEG-200: (a) the whole spectrum (b) Zoom in at the O 1s region (c) Zoom in at the Fe 2p region.

be highlighted that the exact spot of the peaks depends on the history of the samples as well as on the particles size.<sup>36</sup> The peak around  $630.8 \text{ cm}^{-1}$  is characteristic of maghemite.<sup>37</sup> The band at  $1384.4 \text{ cm}^{-1}$  is attributed to some impurity of KBr and shall be neglected. The peak at  $3429.2 \text{ cm}^{-1}$  can be assigned to OH stretching vibrations of the absorbed water, as well as to the OH groups found on the surface of magnetite nanoparticles.<sup>38</sup> The peak at  $1630.7 \text{ cm}^{-1}$  is attributed to O-H bending vibration of water molecules.<sup>29</sup>

### E. X-ray photoelectron spectra

The XPS spectra of samples prepared via PEG-assisted synthesis are illustrated in Fig. 9. Peaks at 1300 eV concerning Mg and traces of Ca and Cl, are common contamination during sample handling. The peak at 530 eV is characteristic of the energy of the anion  $\text{O}^{2-}$  of  $\text{Fe}_2\text{O}_3$ .<sup>39</sup> The broadening of this peak indicates the presence of hydroxides, fact that is consistent with peaks observed at FT-IR and Raman spectra. The characteristic peaks at 724.6 eV and 711 eV concern the binding energy of Fe ( $2p_{1/2}$ ) and the binding energy of the Fe ( $2p_{3/2}$ ) respectively, in addition with the "satellite" peak at 719 eV, indicate the presence of hematite ( $\alpha\text{-Fe}_2\text{O}_3$ ) or maghemite ( $\gamma\text{-Fe}_2\text{O}_3$ ).<sup>40,41</sup> The peak at 285 eV is characteristic C(1s) peak, which cannot be used as indication of PEG presence, since it concerns the inevitable presence of C on the XPS surfaces.

### F. Thermal analysis

TG and DSC curves of the prepared nanoparticles are illustrated in Figure 10. All the curves present a common region of weight loss, accompanied by an endothermic phenomenon at the

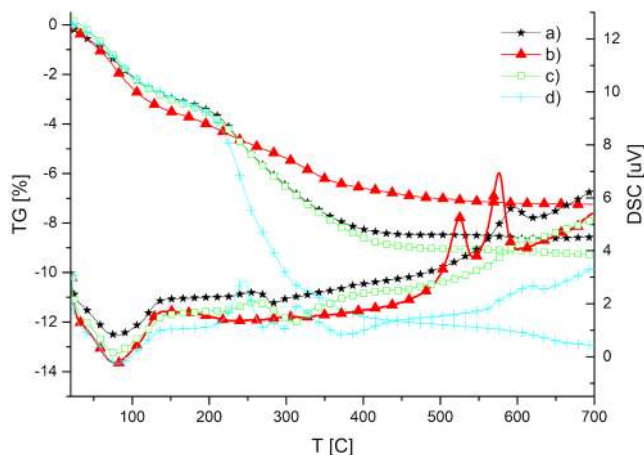


FIG. 10. TG/DSC pattern of nanoparticles prepared in the presence of PEG-200 for 2.5' @400 W using: a) 1.1M ammonia (sample O), b) 0.8M ammonia (sample I), c) 0.5 M ammonia solution (sample C) and d) nanoparticles prepared in the absence of PEG-200 (sample G).

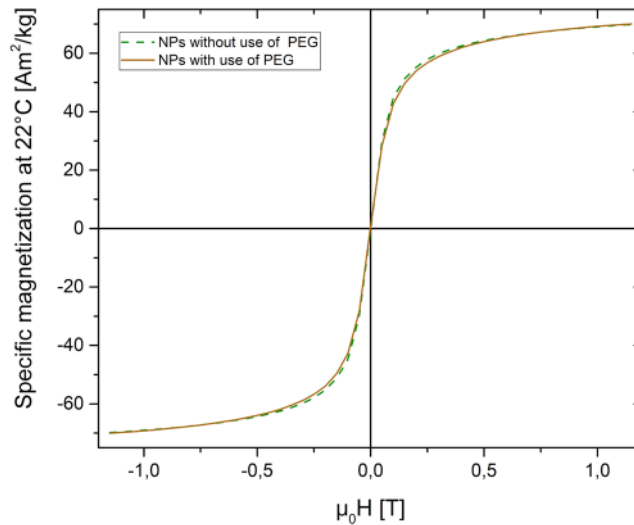


FIG. 11. Representative magnetization curves for nanoparticles prepared in the presence and in the absence of PEG.

temperature range from 25°C to 150°C, which indicates the loss of physically absorbed water. For the nanoparticles prepared without use of PEG (sample B), an additional weight loss is located at 500-600°C indicating the phase transformation to hematite.<sup>42</sup> For the nanoparticles prepared by PEG-assisted synthesis (samples A, C, D) the weight loss at 200-500°C is greater, in comparison with sample B. The main weight losses at 200-350°C are attributed to the decomposition of organic components, which were present on the surface of the nanoparticles.<sup>43</sup> It is observed that the DSC curve, for the nanoparticles prepared using PEG, presents a multistep exothermic peak at 200-350°C, especially for sample D. At this temperature range, the TG curve shows an intense weight loss. These phenomena could be attributed to the deformation of PEG coating. However, it should be mentioned that literature indicates the presence of an endothermic event at 250°C, which is assigned to the dehydration process of possible hydroxides FeO(OH) to hematite.<sup>44</sup>

### G. Magnetic properties

The saturated mass magnetization was determined by vibrating sample magnetometer. Two representative magnetization curves of nanoparticles prepared with and without PEG-assistance are illustrated in Figure 11. It is observed that both sample show similar magnetic behavior and exhibit a saturated mass magnetization of 70 emu g<sup>-1</sup>. Furthermore, the magnetization loop obtained in room temperature illustrates absence of hysteresis and remanence magnetization, which is the main characteristic of super-paramagnetic behavior. Future work is to be devoted in temperature dependent magnetization response in order to observe the critical transition temperature from the ferromagnetic to the super-paramagnetic state, thus allowing for the determination of the anisotropy constant,  $k$ , of the powders.

## IV. DISCUSSION

The produced nanoparticles are all in the phase of magnetite and maghemite, with the ones prepared in the presence of PEG showing larger participation of magnetite (Fig. 1). As shown in Fig. 1, the PEG-assisted prepared nanoparticles are expected to be smaller in size, in comparison with the nanoparticles prepared without the assistance of PEG. The same applies when nanoparticles prepared in the presence of PEG-400, are compared with particles prepared in the presence of PEG-200 (Fig. 2). From Fig. 3 it is concluded that the ammonia concentration, in the range of values that have been tested in this study, do not play significant role on the reaction's evolution. This conclusion applies also for the samples prepared under minimum power for 1 to 5 min and also for the samples prepared under medium microwave power for 2.5 min. All the XRD patterns of the produced

nanoparticles, prepared with the PEG-assisted method, show lower participation of maghemite in comparison with the ones prepared through the PEG-free synthetic route. This phenomenon can be attributed to the sacrificial role of PEG, which protects the nanoparticles from oxidation during the synthetic process. Moreover, samples prepared under microwave heating for 5 min, and samples prepared under maximum microwave power, also show greater participation of maghemite. This observation can be related to a critical point of microwave-assisted heating conditions, which when exceeded PEG fail to protect the nanoparticles from oxidation, since the temperature is high enough to accommodate the oxidation of magnetite to maghemite. It is also essential to mention the noticeable change of color of the samples, from black/dark brown to brown, after their drying. As Hu et.al. showed, drying in the presence of air at 100°C lead to maghemite formation, in contrast to drying in the presence of nitrogen.<sup>45</sup>

From TABLE IV, it is concluded that, nanoparticles prepared in the presence of PEG, keeping constant the rest of parameters, exhibit lower average crystallite size in comparison with the samples prepared in the absence of PEG, regardless the ammonia concentration. This phenomenon can be attributed to the binding role of PEG, which provides a template for rapid nucleation of particles. The reductive effect of  $\beta$ -CD, on the nanoparticles size, is also evident, comparing the last sample with the one prepared under the same conditions, but only in the presence of PEG. In detail, the sample prepared with PEG and  $\beta$ -CD, exhibits smaller nanoparticles size by 7.5 nm. It is also observed that the average crystallite size is greatly affected from the microwave power and the heating time. In particular, the average crystallite size increases when one of the above parameters is increased.

The advantage of the microwave-assisted method, in comparison to other chemical methods, due to its rapid "in core" heating of materials and its selective absorbance from particular chemical bonds, resulting to nano-sized particles, with good uniformity of shape and size is depicted again from the TEM images (Fig. 5). It is also clear, that the PEG-assisted method resulted in nanoparticles of smaller size and narrower size distribution. Concerning the shape of the nanoparticles, both synthetic routes resulted in uniform faceted particles. However, because of the large specific area, high surface energy, and magnetization of the nanoparticles, partial agglomeration was observed, a fact that could also be attributed to lacking *in situ* PEG coating.

Another main advantage of the method described herein, is the ability to coat the nanoparticles with selected molecules, due to the nature of the microwave-assisted heating. Raman spectra failed to offer a clear insight on the nanoparticles coating. Along the same lines, regarding the FTIR results, a clear answer concerning the existence of PEG in the PEG-assisted prepared sample is still not given. The presence of bands around 1115  $\text{cm}^{-1}$  and 1070  $\text{cm}^{-1}$ , on one hand could be attributed to the response of C-O-C etheric bonds,<sup>28</sup> but on the other hand they could be attributed, according to the literature, to the characteristic OH deformation of hydroxides.<sup>36</sup> Therefore, the presence of PEG in the form of coating is still questionable. However, if it does appear as coating, then it is expected to be insufficient in quantity to permit FT-IR and Raman spectroscopy to detect it, also leading to oxidation of the samples during storage, as they come in touch with environmental conditions.

From the XPS results, as presented in Fig. 9, it is concluded that the prepared nanoparticles are surface oxidized to hematite or maghemite to a depth of at least 5 nm. Moreover, taking into consideration the XRD patterns, where hematite was absent, it is safe to assume that XPS indicated the surface oxidation of the nanoparticles to maghemite. In order to evaluate the post-process and post-characterization PEG presence, a more in detail analysis of the carbon peaks is needed. From Fig. 11 the sacrificial role of PEG during oxidation is depicted, as samples A, C and D present the oxidation peaks at higher temperatures, in comparison with sample B. The explanation of thermal analysis presents some difficulties regarding the temperature range 200-350°C. Taking into consideration the possible presence of hydroxides in the XPS and Raman results, part of the endothermic peak is attributed to them. However the comparison of curve B with the rest (Fig. 10), strongly supports the presence of PEG molecules on the surface of the nanoparticles.

From all the above it is safe to conclude that nanoparticles are partially coated with PEG as Raman, FTIR, XPS and TG/DSC analyses indicated. Taking into consideration, that the nanoparticles were prepared in a domestic oven, the method is very promising for *in situ* coating of nanoparticles when

a frequency-power-environment tuned microwave oven is used, where all these conditions, namely frequency, power and gas atmosphere are under control.

Regarding the magnetic measurements, the value of magnetization indicates the strong participation of magnetite in the prepared nano-powders, since typical value of  $M_s$  for magnetite is 85-100 emu g<sup>-1</sup>, whereas for maghemite is only 56 emu g<sup>-1</sup>. Moreover, it is known that the effective saturation magnetization is reduced compared to the bulk material.<sup>30,35,46</sup>

## V. CONCLUSIONS

In conclusion, a microwave-assisted method for the synthesis of magnetite and maghemite nanoparticles with well-controlled size, high crystallinity and good magnetic properties, under short reaction time has been developed. The process is simple, time-saving and low energy-consuming due to the advantages of the microwave irradiation. It is noticed that microwave power and heating time are the main parameters controlling the size of the nanoparticles and the presence of maghemite, whereas ammonia concentration does not strongly affected it. The PEG-assisted synthetic route showed better results in terms of particle size (8.5 nm ± 0.5 nm) and oxidation resistance. The obtained results indicate the presence of partial polymeric coating. However, the quality of the bond between the polymer and the nanoparticles cannot be evaluated.

## ACKNOWLEDGMENTS

Acknowledgements are due to the Alexander S. Onassis Public Benefit Foundation for the scholarship supporting E.A.

This paper is part of "VALUEMAG" project that has received funding from the Bio Based Industries Joint Undertaking under the European Union's Horizon 2020 research and innovation programme under grant agreement No 745695.

Acknowledgements are also due to Dr. Peter Svec, Slovak Academy of Sciences for contacting transmission electron microscopy studies, to Dr. Spyros Diplas, Sintef, Norway, for contacting X-Ray Photoelectron Spectroscopy studies and to Dr. Kostas Efthimiadis, Aristotle University of Thessaloniki for contacting vibrating sample magnetometer studies.

- <sup>1</sup> Q. A. Pankhurst, J. Connolly, S. K. Jones, and J. Dobson, "Applications of magnetic nanoparticles in biomedicine," *J Phys Appl Phys* **36**, R167–R181 (2003).
- <sup>2</sup> D. K. Kim, "Characterization and MRI study of surfactant-coated superparamagnetic nanoparticles administrated into the rat brain," *J Magn Magn Mater* **225**, 256–261 (2001).
- <sup>3</sup> A. K. Gupta and M. Gupta, "Synthesis and surface engineering of iron oxide nanoparticles for biomedical applications," *Biomaterials* **26**(18), 3995–4021 (2005).
- <sup>4</sup> J. Devkota *et al.*, "A novel approach for detection and quantification of magnetic nanomarkers using a spin valve GMR-integrated microfluidic sensor," *RSC Adv* **5**(63), 51169–51175 (2015).
- <sup>5</sup> G. Kokkinis, M. Jamalieh, F. Cardoso, S. Cardoso, F. Keplinger, and I. Giouroudi, "Magnetic-based biomolecule detection using giant magnetoresistance sensors," *J. Appl. Phys.* **117**(17), 17B731 (2015).
- <sup>6</sup> C. P. Gooneratne, O. Yassine, I. Giouroudi, and J. Kosel, "Selective manipulation of superparamagnetic beads by a magnetic microchip," *IEEE Trans. Magn.* **49**(7), 3418–3421 (2013).
- <sup>7</sup> C. Gooneratne, I. Giouroudi, and J. Kosel, "A planar conducting micro-loop structure for transportation of magnetic beads: An approach towards rapid sensing and quantification of biological entities," *Sens. Lett.* **10**, 769–773 (2012).
- <sup>8</sup> T. J. Daou *et al.*, "Phosphate adsorption properties of magnetite-based nanoparticles," *Chem. Mater.* **19**(18), 4494–4505 (2007).
- <sup>9</sup> T. Muraliganth, A. Vadivel Murugan, and A. Manthiram, "Facile synthesis of carbon-decorated single-crystalline Fe<sub>3</sub>O<sub>4</sub> nanowires and their application as high performance anode in lithium ion batteries," *Chem. Commun.* **47**, 7360 (2009).
- <sup>10</sup> I. Giouroudi, J. Kosel, and C. Scheffer, "BioMEMS in diagnostics: A review and recent developments," *Recent Pat. Eng.* **2**(2), 114–121 (2008).
- <sup>11</sup> V. Iannotti *et al.*, "Magnetic anisotropy in Ni–Si nanoparticle films produced by ultrashort pulsed laser deposition," *J. Magn. Magn. Mater.* **320**(20), e594–e598 (2008).
- <sup>12</sup> M. Mahdavi *et al.*, "Synthesis, surface modification and characterisation of biocompatible magnetic iron oxide nanoparticles for biomedical applications," *Molecules* **18**(7), 7533–7548 (2013).
- <sup>13</sup> N. M. Gribanov, E. E. Bibik, O. V. Buzunov, and V. N. Naumov, "Physico-chemical regularities of obtaining highly dispersed magnetite by the method of chemical condensation," *J. Magn. Magn. Mater.* **85**, 7–10 (1990).
- <sup>14</sup> N. R. Jana, Y. Chen, and X. Peng, "Size and shape-controlled magnetic (Cr, Mn, Fe, Co, Ni) oxide nanocrystals via a simple and general approach," *Chem. Mater.* **16**, 3931–3935 (2004).
- <sup>15</sup> J. Rockenberger, E. C. Scher, and A. P. Alivisatos, "A new nonhydrolytic single-precursor approach to surfactant-capped nanocrystals of transition metal oxides," *J. Am. Chem. Soc.* **121**, 11595–11596 (1999).

- <sup>16</sup> C. Okoli, M. Sanchez-Dominguez, M. Boutonnet *et al.*, "Comparison and functionalization study of microemulsion-prepared magnetic iron oxide nanoparticles," *Langmuir* **28**, 8479–8485 (2012).
- <sup>17</sup> K. He, C.-Y. Xu, L. Zhen, and W.-Z. Shao, "Hydrothermal synthesis and characterization of single-crystalline Fe<sub>3</sub>O<sub>4</sub> nanowires with high aspect ratio and uniformity," *Mater. Lett.* **61**(14-15), 3159–3162 (2007).
- <sup>18</sup> W. Wu *et al.*, "Single-crystalline- $\alpha$ -Fe<sub>2</sub>O<sub>3</sub> nanostructures: Controlled synthesis and high-index plane-enhanced photodegradation by visible light," *J Mater Chem A* **23**, 6888–6894 (2013).
- <sup>19</sup> C. O. Kappe, "Controlled microwave heating in modern organic synthesis," *Angew. Chem. Int. Ed.* **43**(46), 6250–6284 (2004).
- <sup>20</sup> X. H. Zhu and Q. M. Hang, "Microscopical and physical characterization of microwave and microwave-hydrothermal synthesis products," *Micron* **44**, 21–44 (2013).
- <sup>21</sup> Y. B. Kholam *et al.*, "Microwave hydrothermal preparation of submicron-sized spherical magnetite (Fe<sub>3</sub>O<sub>4</sub>) powders," *Mater. Lett.* **56**(4), 571–577 (2002).
- <sup>22</sup> T. Caillot, D. Aymes, D. Stuerger, N. Viart, and G. Pourroy, "Microwave flash synthesis of iron and magnetite particles by disproportionation of ferrous alcoholic solutions," *J. Mater. Sci.* **37**(23), 5153–5158 (2002).
- <sup>23</sup> H. Hu *et al.*, "Unique role of ionic liquid in microwave-assisted synthesis of monodisperse magnetite nanoparticles," *Chem. Commun.* **46**(22), 3866 (2010).
- <sup>24</sup> R. Y. Hong, T. T. Pan, and H. Z. Li, "Microwave synthesis of magnetic Fe<sub>3</sub>O<sub>4</sub> nanoparticles used as a precursor of nanocomposites and ferrofluids," *J. Magn. Magn. Mater.* **303**(1), 60–68 (2006).
- <sup>25</sup> P. Russo *et al.*, "Ultrafine magnetite nanopowder: Synthesis, characterization, and preliminary use as filler of polymethylmethacrylate nanocomposites," *J. Nanotechnol.* **2012**.
- <sup>26</sup> L. Gonzalez-Moragas, S.-M. Yu, N. Murillo-Cremaes, A. Laromaine, and A. Roig, "Scale-up synthesis of iron oxide nanoparticles by microwave-assisted thermal decomposition," *Chem. Eng. J.* **281**, 87–95 (2015).
- <sup>27</sup> S. Komarneni *et al.*, "Magnetite syntheses from room temperature to 150°C with and without microwaves," *Ceram. Int.* **38**(3), 2563–2568 (2012).
- <sup>28</sup> W.-W. Wang, Y.-J. Zhu, and M.-L. Ruan, "Microwave-assisted synthesis and magnetic property of magnetite and hematite nanoparticles," *J. Nanoparticle Res.* **9**(3), 419–426 (2007).
- <sup>29</sup> A. B. Savić *et al.*, "Tailoring of magnetite powder properties for enhanced phosphate removal: Effect of PEG addition in the synthesis process," *Powder Technol.* **301**, 511–519 (2016).
- <sup>30</sup> F. A. Harraz, "Polyethylene glycol-assisted hydrothermal growth of magnetite nanowires: Synthesis and magnetic properties," *Phys. E Low-Dimens. Syst. Nanostructures* **40**(10), 3131–3136 (2008).
- <sup>31</sup> J. Zhang and P. X. Ma, "Cyclodextrin-based supramolecular systems for drug delivery: Recent progress and future perspective," *Adv. Drug Deliv. Rev.* **65**(9), 1215–1233 (2013).
- <sup>32</sup> M. Hanesch, "Raman spectroscopy of iron oxides and (oxy)hydroxides at low laser power and possible applications in environmental magnetic studies," *Geophys. J. Int.* **177**(3), 941–948 (2009).
- <sup>33</sup> D. L. Faria, V. Silva, and M. T. Oliveira, "Raman microspectroscopy of some iron oxides and oxyhydroxides," *J. Raman Spectrosc.* **28**, 873–878 (1997).
- <sup>34</sup> O. N. Shebanova and P. Lazor, "Raman study of magnetite (Fe<sub>3</sub>O<sub>4</sub>): Laser-induced thermal effects and oxidation," *J. Raman Spectrosc.* **34**(11), 845–852 (2003).
- <sup>35</sup> M. F. Tai, C. W. Lai, and S. B. Abdul Hamid, "Facile synthesis polyethylene glycol coated magnetite nanoparticles for high colloidal stability," *J. Nanomater.* **2016**, 1–7.
- <sup>36</sup> T. Koutzarova, S. Kolev, C. Ghelev, D. Paneva, and I. Nedkov, "Microstructural study and size control of iron oxide nanoparticles produced by microemulsion technique," *Phys. Status Solidi C* **3**(5), 1302–1307 (2006).
- <sup>37</sup> M. A. Willard, L. K. Kurihara, E. E. Carpenter, S. Calvin, and Harris, *Encyclopedia of Nanoscience and Nanotechnology*, vol. 1. American Scientific Publishers, 2004.
- <sup>38</sup> G. Nabiyouni, M. Julaei, D. Ghanbari, P. C. Aliabadi, and N. Safaie, "Room temperature synthesis and magnetic property studies of Fe<sub>3</sub>O<sub>4</sub> nanoparticles prepared by a simple precipitation method," *J. Ind. Eng. Chem.* **21**, 599–603 (2015).
- <sup>39</sup> S. Basavaraja, H. Vijayanand, A. Venkataraman, U. P. Deshpande, and T. Shripathi, "Characterization of  $\gamma$ -Fe<sub>2</sub>O<sub>3</sub> nanoparticles synthesized through self-propagating combustion route," *Synth. React. Inorg. Met.-Org. Nano-Met. Chem.* **37**(6), 409–412 (2007).
- <sup>40</sup> T. Yamashita and P. Hayes, "Analysis of XPS spectra of Fe<sup>2+</sup> and Fe<sup>3+</sup> ions in oxide materials," *Appl. Surf. Sci.* **254**(8), 2441–2449 (2008).
- <sup>41</sup> M. C. Biesinger, B. P. Payne, A. P. Grosvenor, L. W. M. Lau, A. R. Gerson, and R. S. C. Smart, "Resolving surface chemical states in XPS analysis of first row transition metals, oxides and hydroxides: Cr, Mn, Fe, Co and Ni," *Appl. Surf. Sci.* **257**(7), 2717–2730 (2011).
- <sup>42</sup> T. J. Daou *et al.*, "Hydrothermal synthesis of monodisperse magnetite nanoparticles," *Chem. Mater.* **18**(18), 4399–4404 (2006).
- <sup>43</sup> V. Panwar, P. Kumar, A. Bansal, S. S. Ray, and S. L. Jain, "PEGylated magnetic nanoparticles (PEG@Fe<sub>3</sub>O<sub>4</sub>) as cost effective alternative for oxidative cyanation of tertiary amines via CH activation," *Appl. Catal. Gen.* **498**, 25–31 (2015).
- <sup>44</sup> M. Stoia, A. Tamas, G. Rusu, and J. Morosanu, "Synthesis of magnetic iron oxides from ferrous sulfate and substitute amines," *Stud. Univ. Babeş-Bolyai Chem.* **61**(4) (2016).
- <sup>45</sup> L. Hu, A. Percheron, D. Chaumont, and C.-H. Brachais, "Microwave-assisted one-step hydrothermal synthesis of pure iron oxide nanoparticles: Magnetite, maghemite and hematite," *J. Sol-Gel Sci. Technol.* **60**(2), 198–205 (2011).
- <sup>46</sup> S. A. Kulkarni, P. S. Sawadh, P. K. Palei, and K. K. Kokate, "Effect of synthesis route on the structural, optical and magnetic properties of Fe<sub>3</sub>O<sub>4</sub> nanoparticles," *Ceram. Int.* **40**(1), 1945–1949 (2014).